Advances in Simulation of High Brightness/High Intensity Beams

Ji Qiang

Accelerator Modeling Program
Lawrence Berkeley National Laboratory

13th International Computational Accelerator Physics Conference

Oct. 20-24, Key West, Florida, USA, 2018

BERKELEY LAB | U.S. DEPARTMENT OF ENERGY | Office of Science | ACCELERATOR TECHNOLOGY & APPLIED PHYSICS DIVISION | ATAP

High Brightness Electron Beam Based X-Ray FEL Light Sources Provide Great Opportunity for Scientific Discovery

Natural and Artificial Photosynthesis

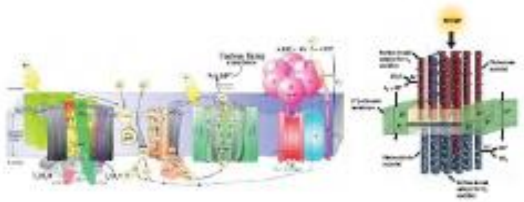

Fundamental Charge Dynamics

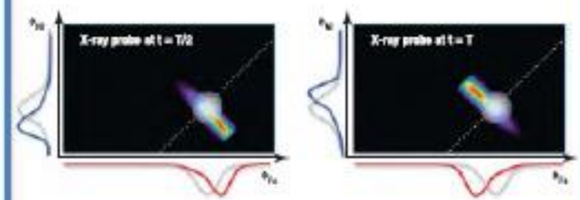

Advanced Combustion Science

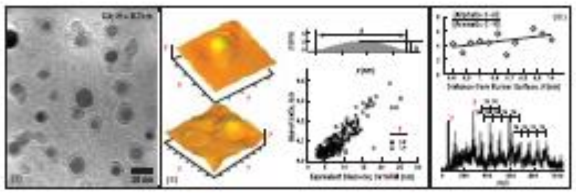

Catalysis

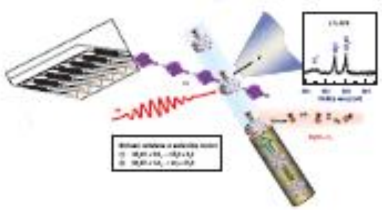

Nanoscale Materials Nucleation

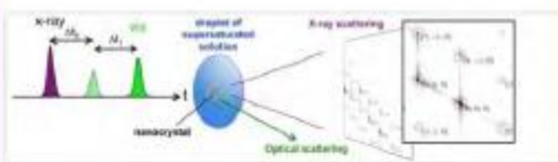

Dynamic Nanoscale Heterogeneity

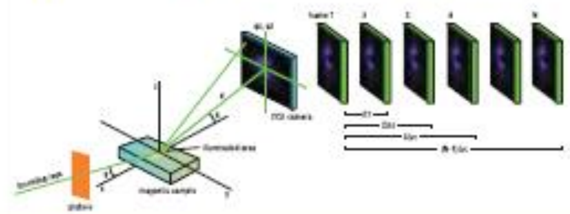

Quantum Materials

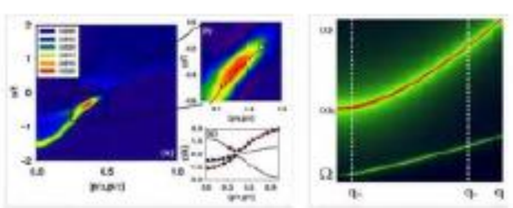

Nanoscale Spin and Magnetization

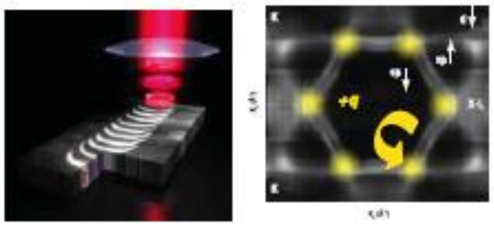

Bioimaging: Structure-to-Function

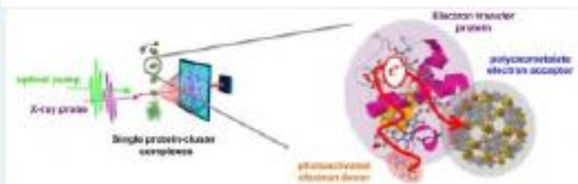

Courtesy of R. Scholenlein

The FEL Cost and Performance Critically Depend on Electron Beam Quality

- **Electron beam emittance ε**

$$\frac{\varepsilon_n}{\gamma} \approx \frac{\lambda_{x-ray}}{4\pi} \qquad \lambda_{x-ray} = \frac{\lambda_{undulator}}{2\gamma^2}\left(1+\frac{K^2}{2}\right)$$

- **Peak current I_{peak}**

$$P_{sat} \approx 1.6\rho\left(\frac{L_{G,1D}}{L_G}\right)^2 P_{b,pk} \qquad P_{b,pk} = I_{pk}\,\gamma\, mc^2/e$$

$$\rho = \left(\frac{1}{16}\frac{I_{pk}}{I_A}\frac{K^2[JJ]^2\lambda_u^2}{4\pi^2\gamma^3\sigma_x^2}\right)^{1/3}$$

- **Gain length**

$$L_{G0} = \frac{\lambda_u}{4\pi\sqrt{3}\rho}$$

- **Energy spread σ_E**

$$\Delta\omega = \frac{2\sigma_\gamma/\gamma}{\lambda_r}c$$

Ideal electron beam:
- high peak current
- small energy spread
- small emittance

Microbunching Instability in Accelerator Degrades Electron Beam Quality

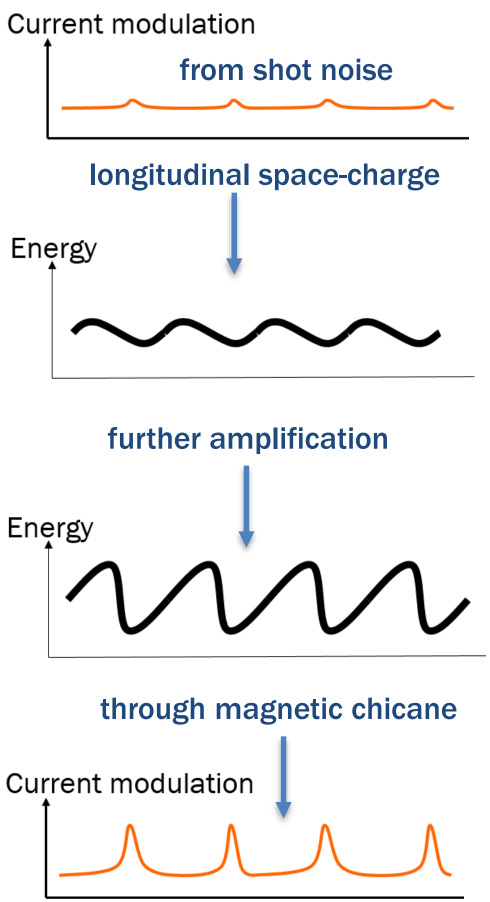

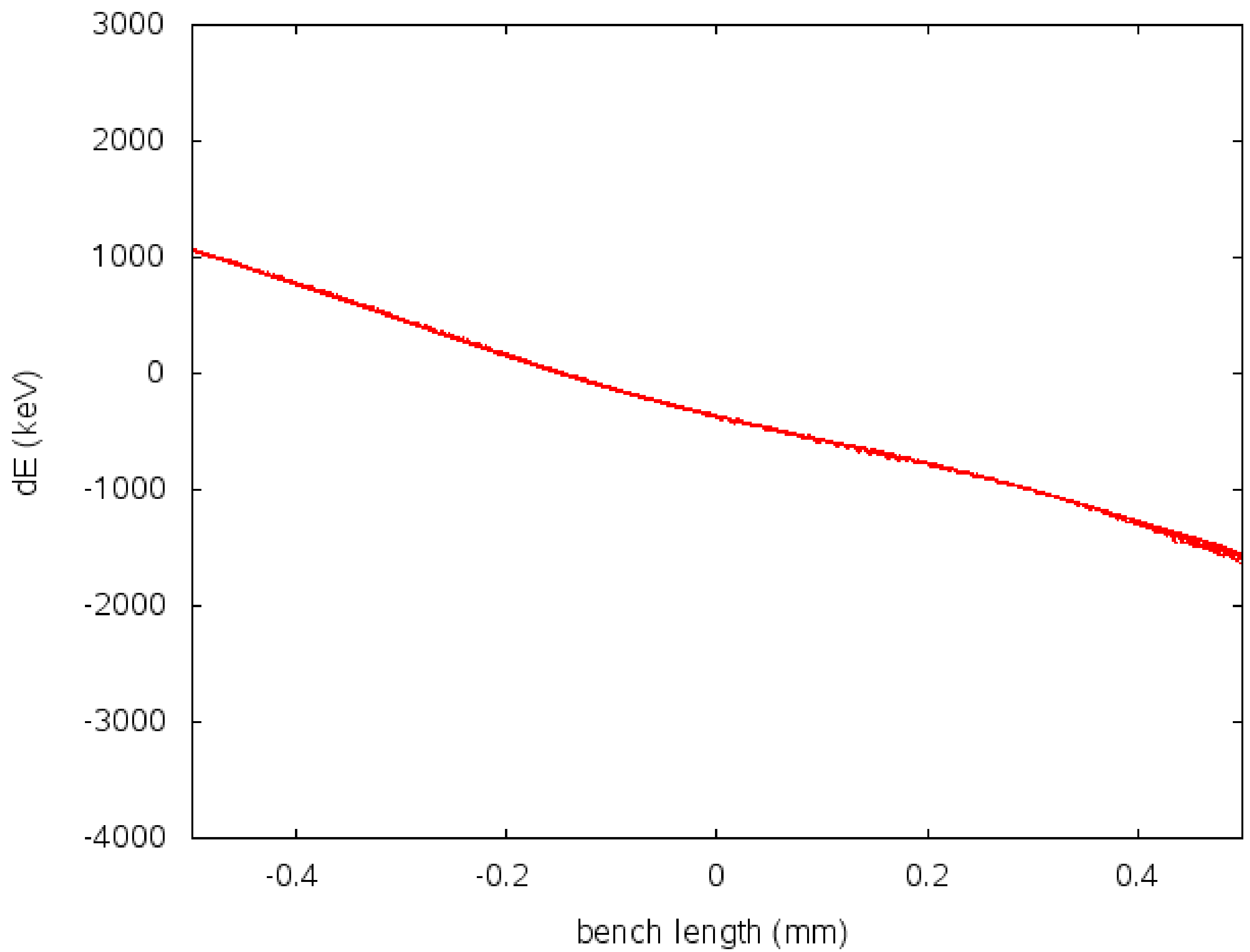

No Tuning Factor Used in Start-to-End Beam Dynamics Simulation of the LCLS Microbunching Experiments

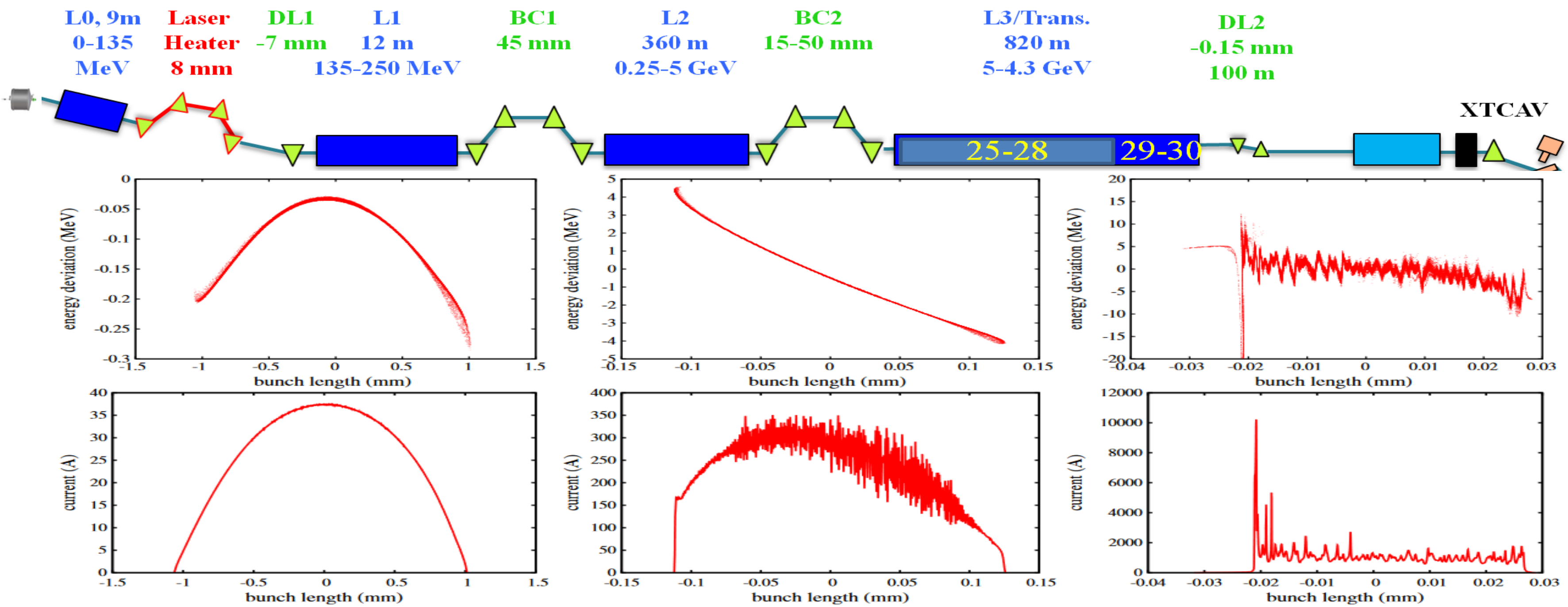

•The multi-physics simulation model includes:

- 1 electron – 1 macroparticles
- MAD lattice input file
- self-consistent 3D space-charge effects
- 1D CSR effects, ISR effects
- structure and resistive wall wakefields
- 5th order single particle tracking

J. Qiang et al., Phys. Rev. Accel. Beams 20, 054402 (2017).

Shot-Noise Driven Microbunching Instability Can Be Reproduced: Benchmark IMPACT Simulations against LCLS Measurements (1)

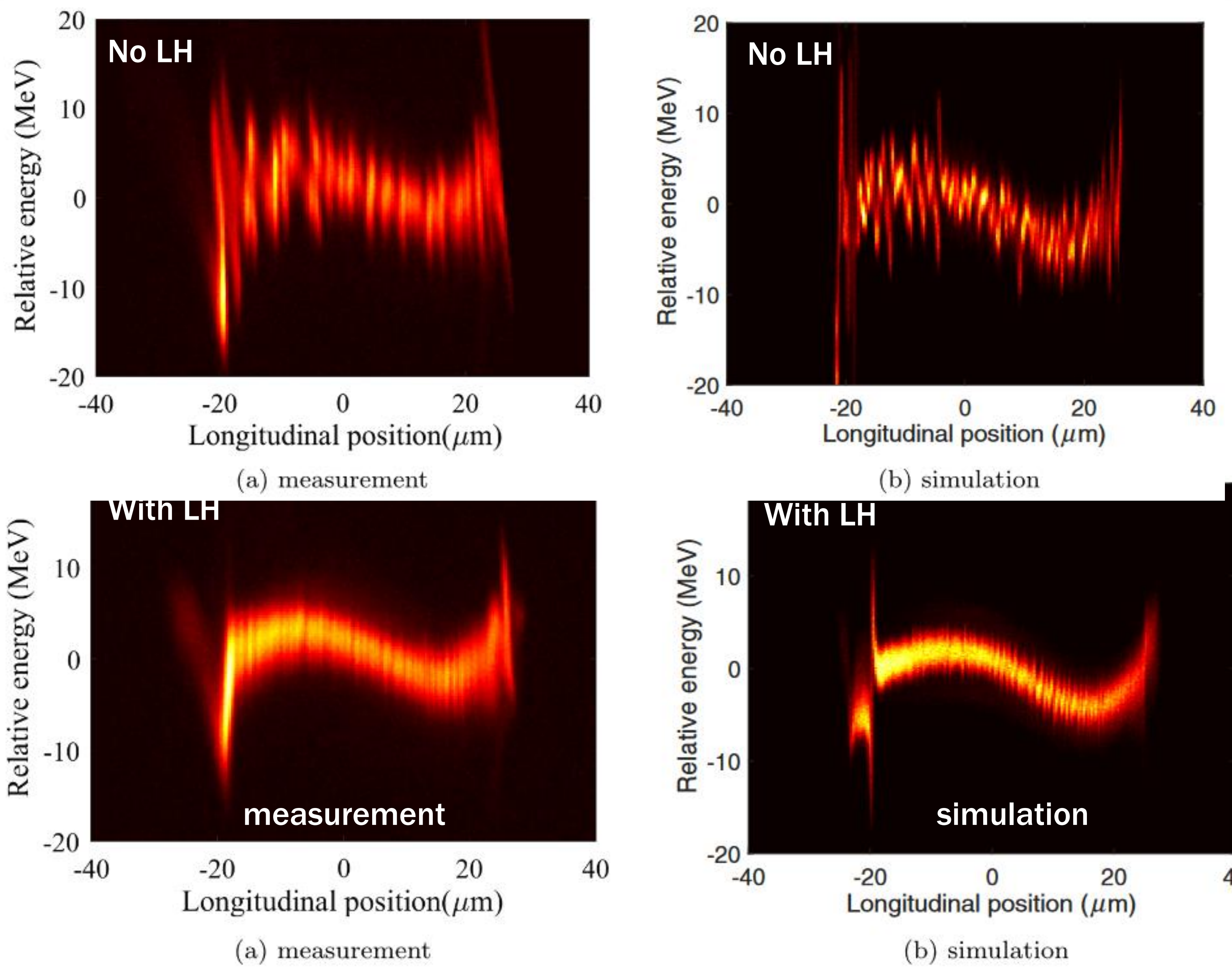

Shot-Noise Driven Microbunching Instability Can Be Reproduced: Benchmark IMPACT Simulations against LCLS Measurements (2)

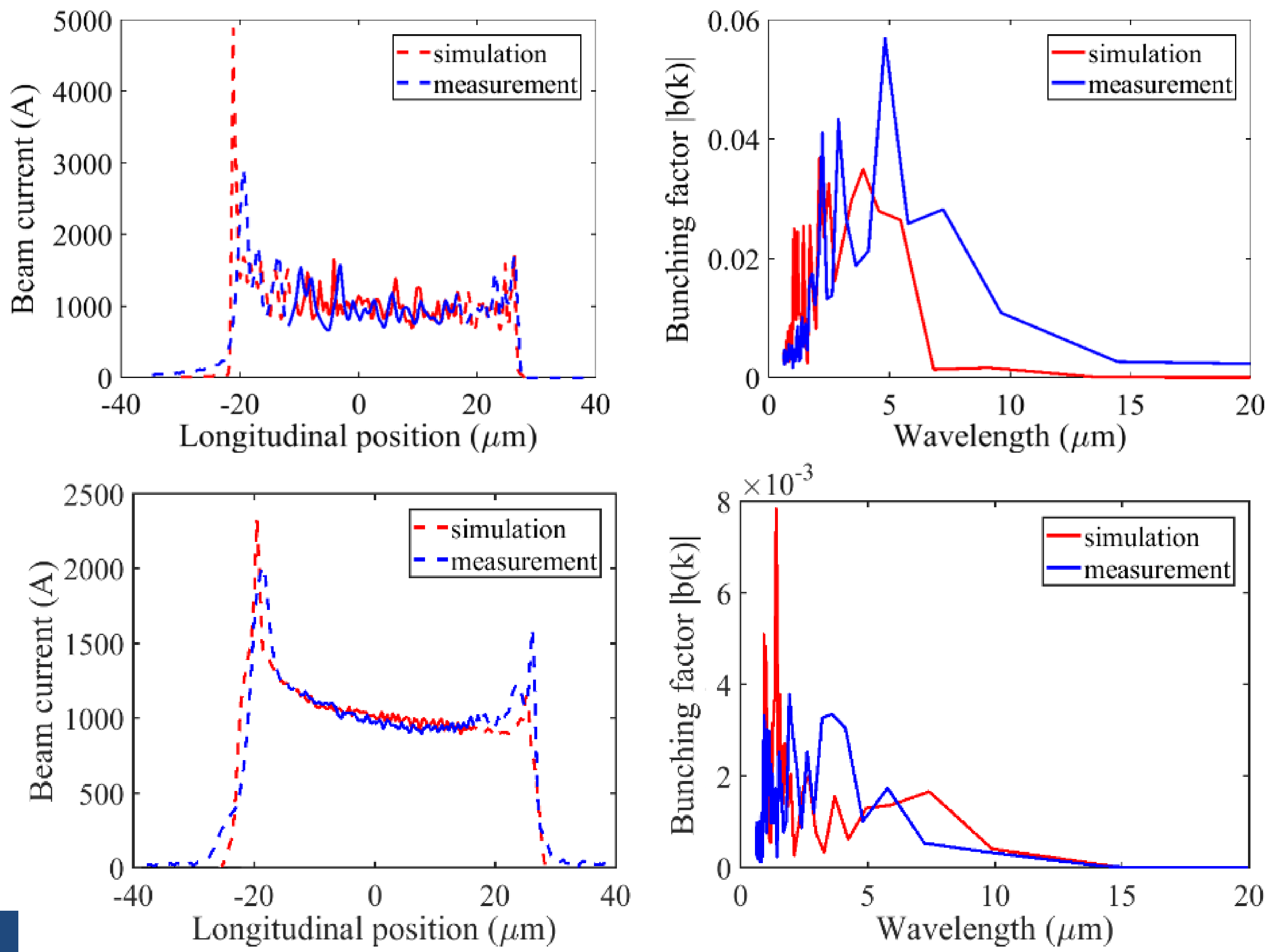

(a) current profile (b) bunching factor

Accelerator Global Parameter Optimization

Global Start-to-End Beam Dynamics Optimization Is Needed to Achieve the “Best” Electron Beam Quality

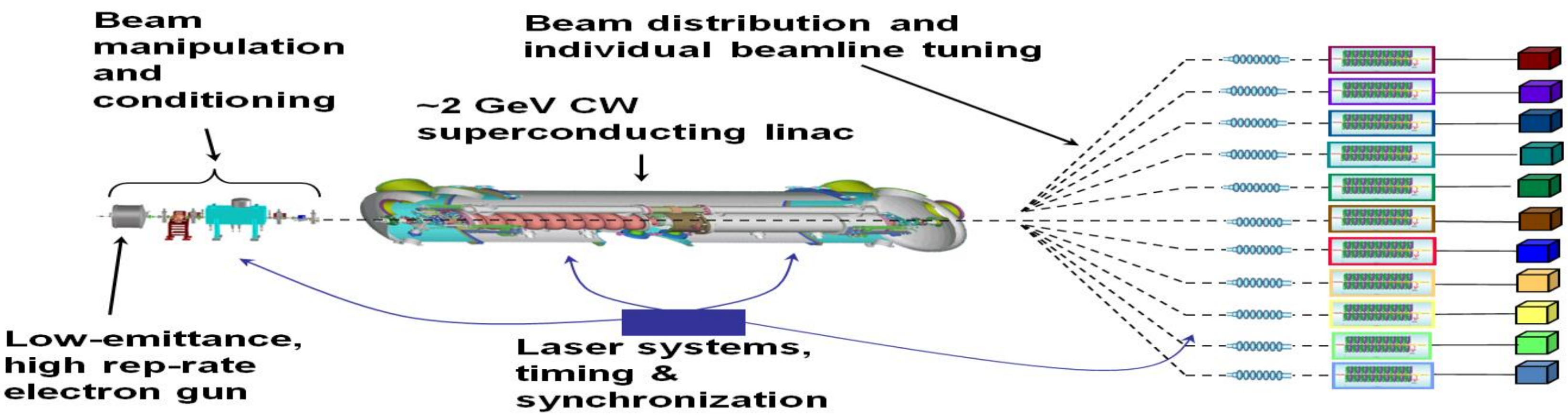

Ref: J. Corlett et al., 2013

- previous studies were done with injector and linac optimization separately
- optimizing the linac using the best-performing solution from the injector does not guarantee the best solution at the end of the accelerator.
- local optima may exist given the high dimension of search space
- global optimization method is needed to avoid local optimal solutions
- global start-to-end simulation is needed to allow all machine control parameters to vary simultaneously.

Global Optimization Using a Stochastic Evolutionary Method to Overcome Local Optimal Solution

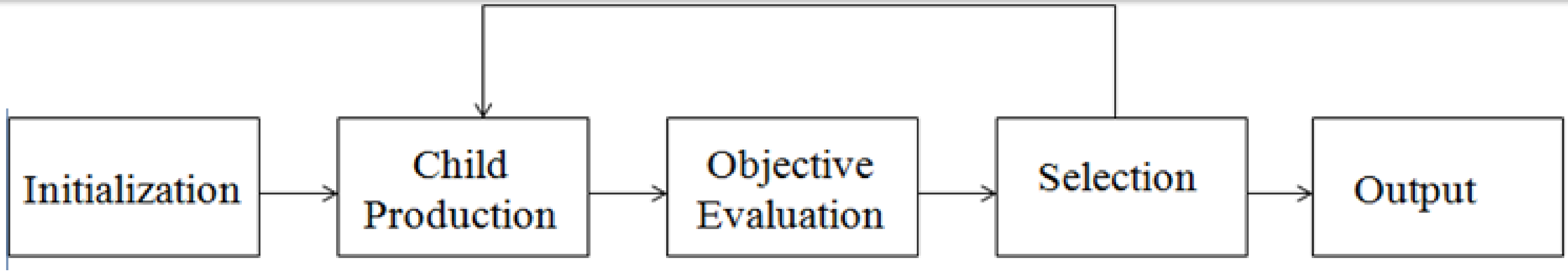

Differential Evolution Algorithm:

- Stochastic, population-based evolutionary optimization algorithm
- Easy to implement and to extend to multi-processor
- DE has been shown to be effective on a large range of classic optimization problems
  - In a comparison by Storn and Price in 1997 DE was more efficient than simulated annealing and genetic algorithms
  - Ali and Torn (2004) found that DE was both more accurate and more efficient than controlled random search
  - In 2004 Lampinen and Storn demonstrated that DE was more accurate than several other optimization methods including four genetic algorithms, simulated annealing and evolutionary programming

R. Storn and K. Price, Journal of Global Optimization 1a1:341-359, (1997).

The New Variable Population External Storage Multi-Objective Algorithm Shows Faster Convergence than the Popular NSGA-II

$$f_1(\mathbf{x}) = x_1 \qquad x_1 \in [0,1]$$

$$f_2(\mathbf{x}) = g(\mathbf{x})\left[1 - (x_1/g(\mathbf{x}))^2\right] \qquad x_i = 0,$$

$$g(\mathbf{x}) = 1 + 9\left(\sum_{i=2}^{n} x_i\right)/(n-1) \qquad i = 2, \ldots, n$$

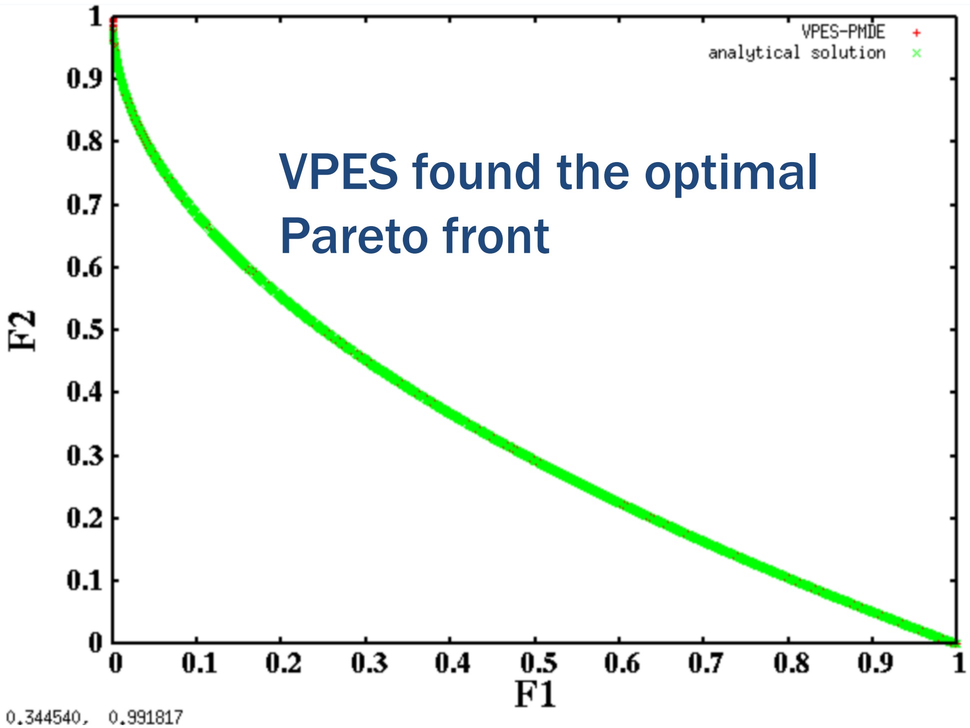

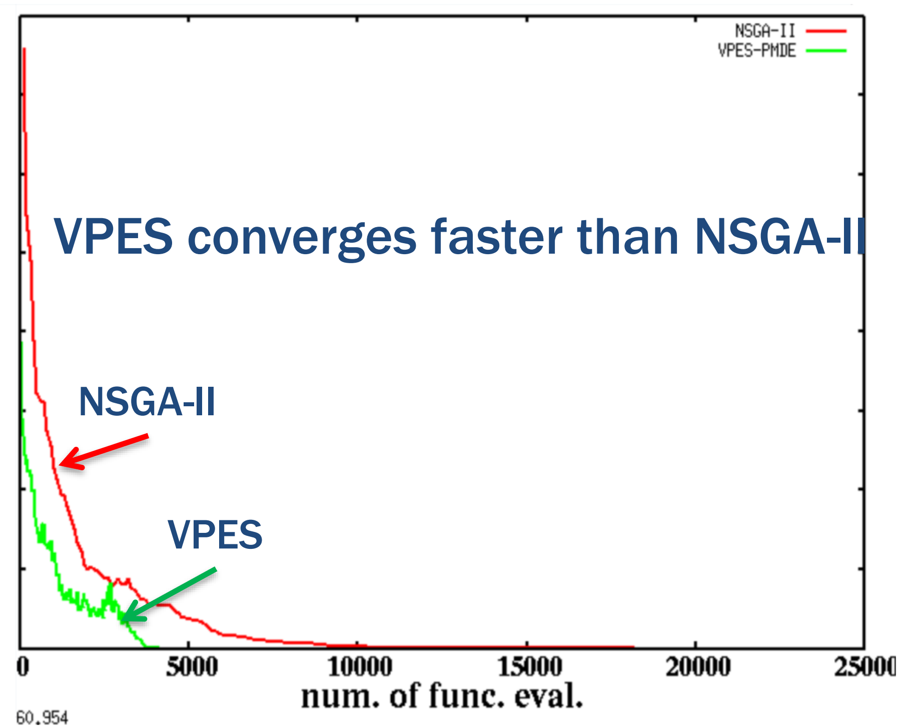

Integration of Self-Consistent Beam Dynamics Simulation Using the IMPACT Code with the New Optimization Algorithm for Global Machine Design Optimization

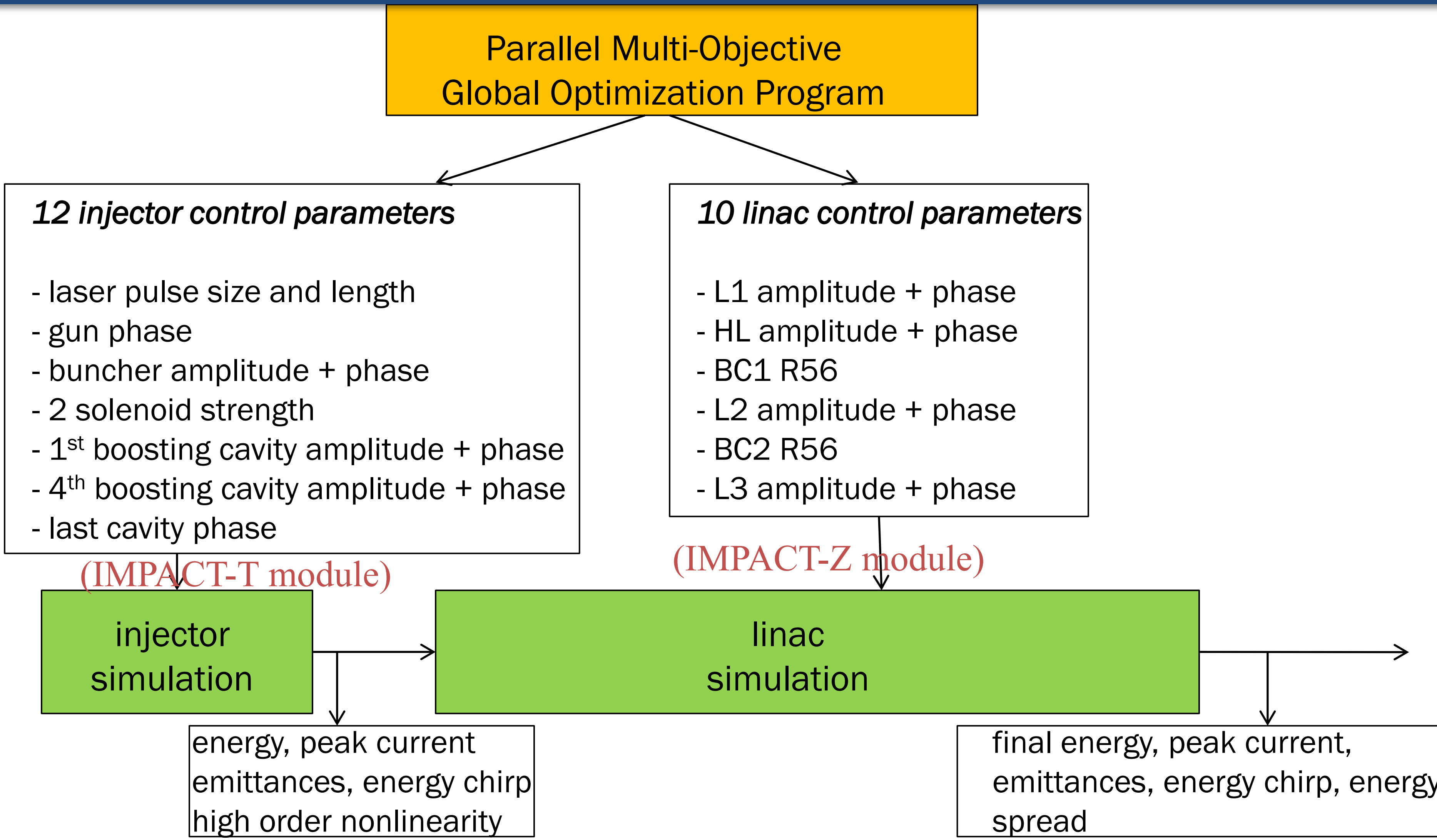

Global Optimization Significantly Improves Accelerator Performance in the LCLS-II Design Application (20 pC Charge)

Pareto front in the Injector Optimization

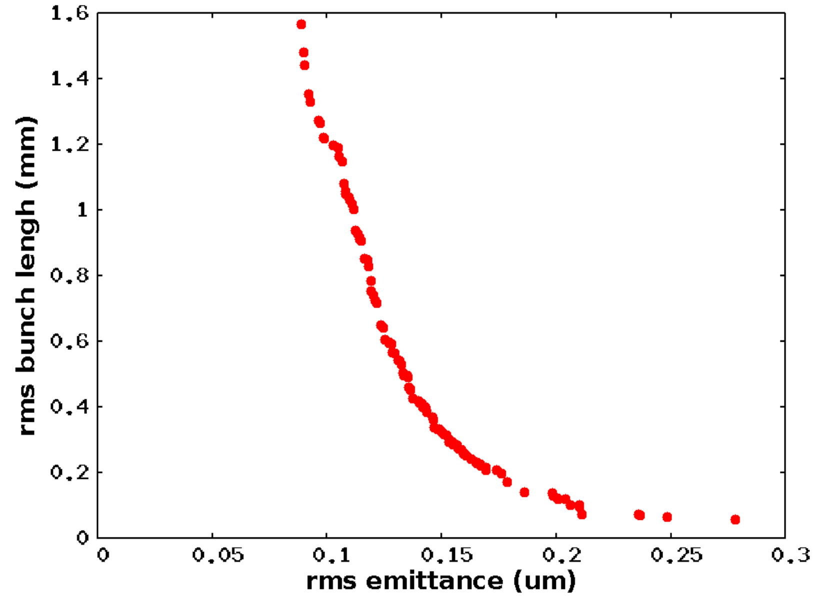

22 Control Parameters:
- 12 in the injector
- 10 in the linac

final Pareto front solutions

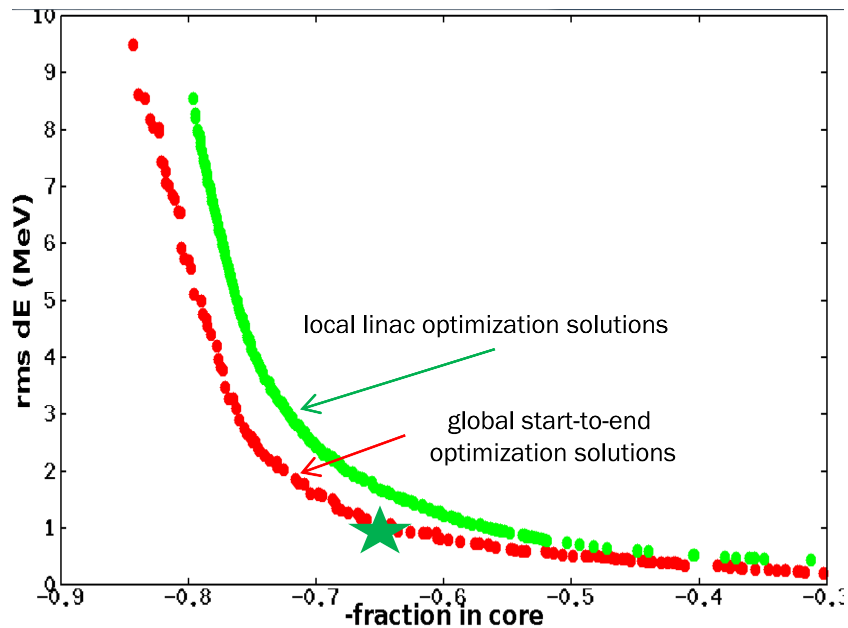

➢ Global optimization shows significantly better solutions than the local optimization

Global Optimization Improves Final Electron Beam Quality and Results in 50% X-Ray Radiation Energy Improvement (20pC)

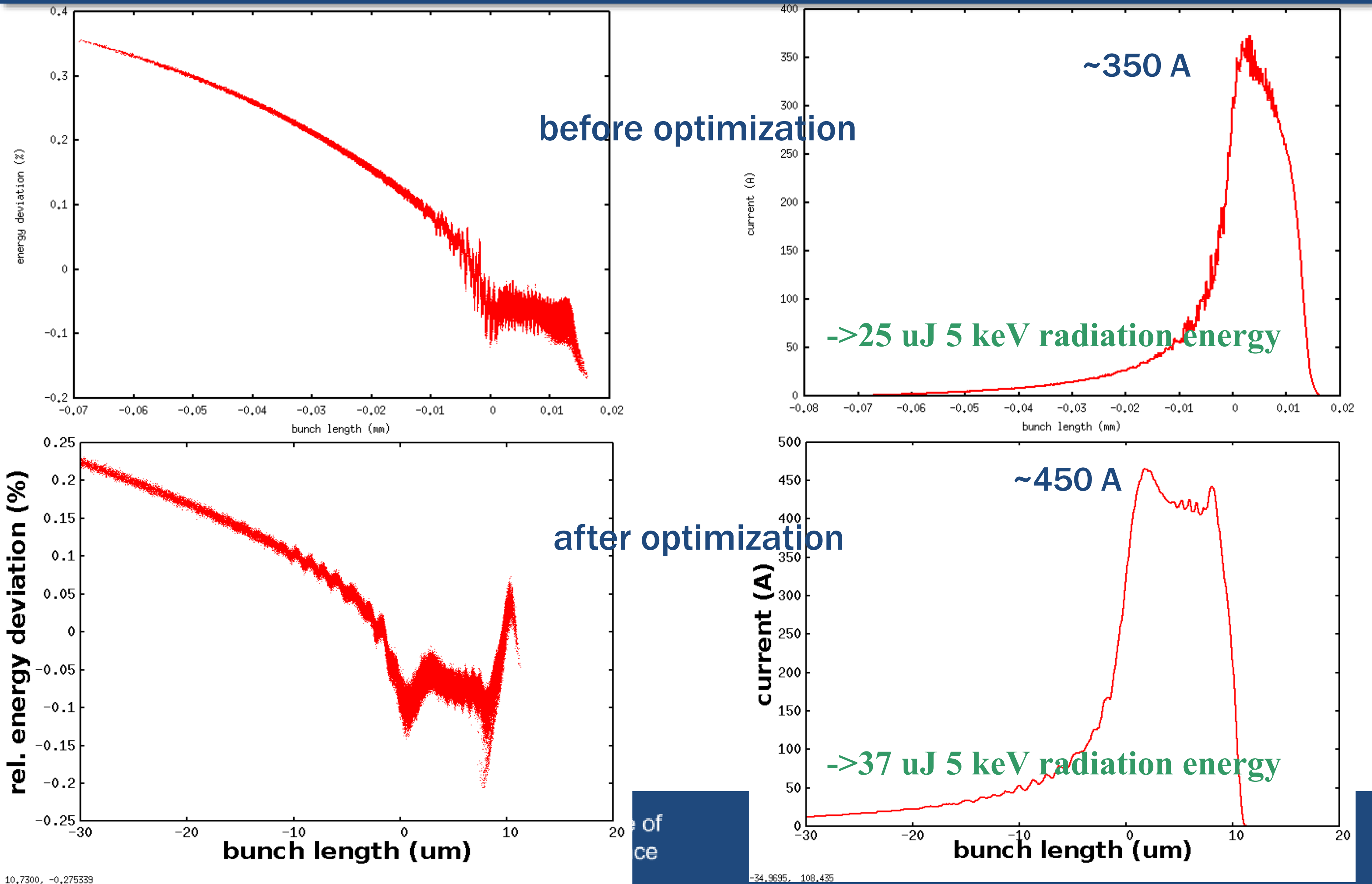

Nonlinear Space-Charge Effects in High Intensity Proton Beams Need High Fidelity Simulation

- **High intensity proton beams are used in:**
  - **Injector for high energy colliders**
  - **Driver for neutrino productions**
  - **Driver for spallation neutron sources**
  - **Driver for nuclear energy production**
- Space-charge effects cause beam quality degradation and potential particle loss in high intensity accelerators
  - Space-charge effects drive coherent instability
  - Space-charge effects cause halo formation
  - Space-charge effects drive and enhance nonlinear resonance
- Reliable self-consistent simulations are needed to handle the nonlinear space-charge effects
  - A fully self-consistent symplectic space-charge model with numerical filtering improves simulation accuracy

Contrast of Non-Symplectic and Symplectic Integrator

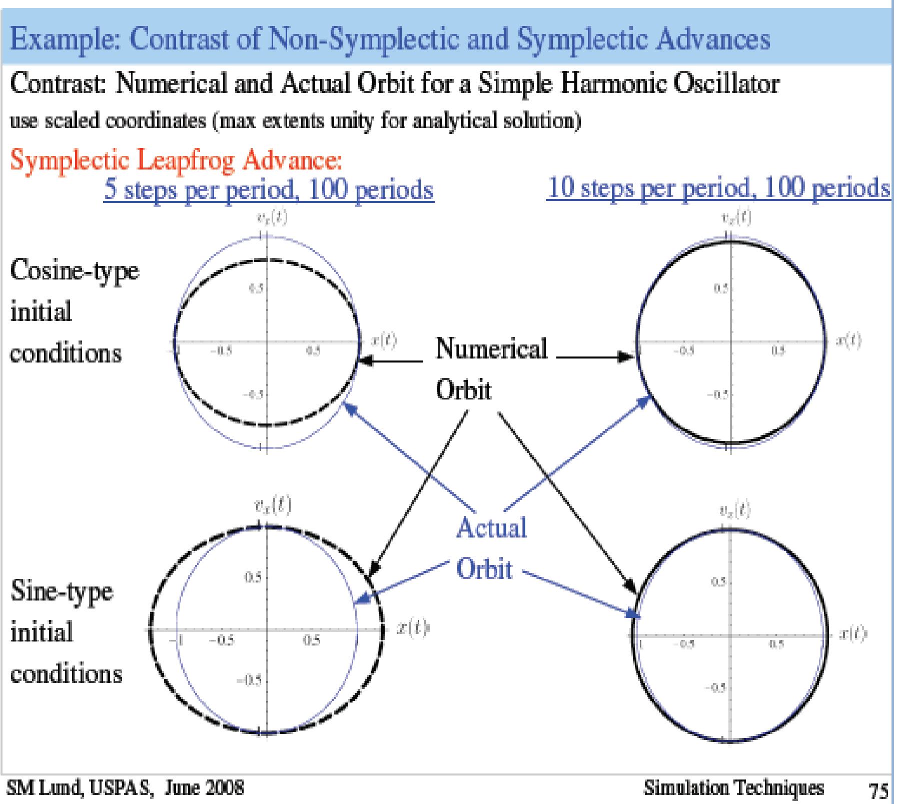

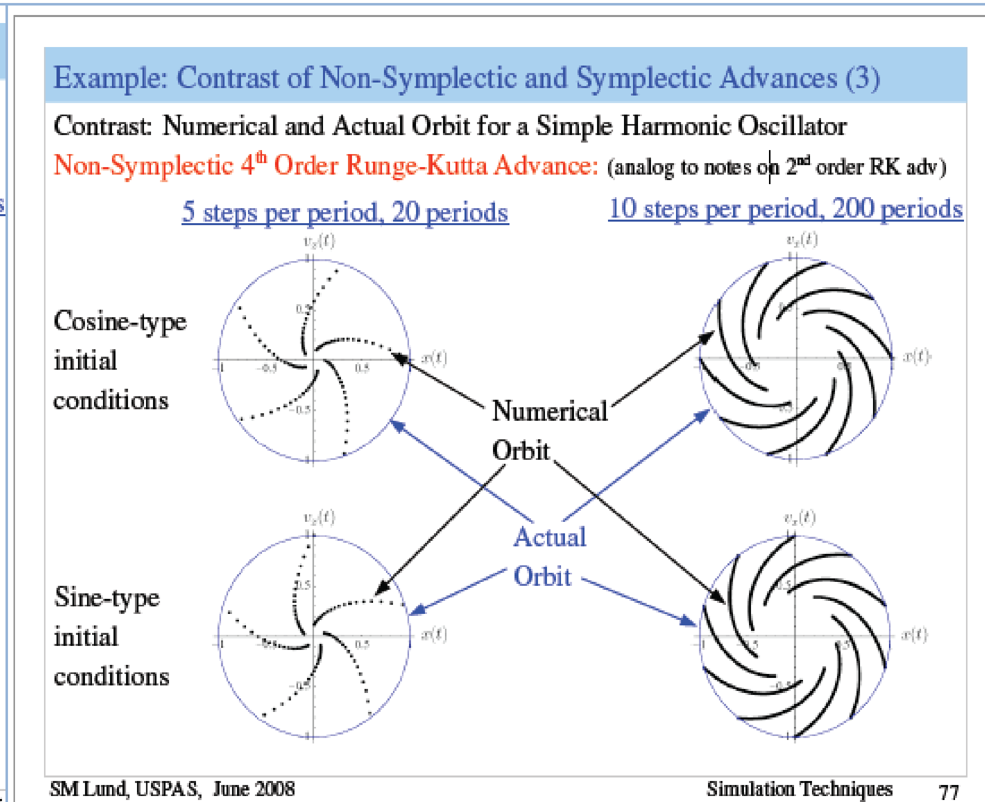

Courtesy of S. Lund

A Symplectic Multi-Particle Tracking Model (1)

Multi-particle Hamiltonian $H(\mathbf{r}_1, \mathbf{r}_2, \cdots, \mathbf{p}_1, \mathbf{p}_2, \cdots, s)$

$$H = \sum_i \mathbf{p}_i^2/2 + \frac{1}{2}\sum_i \sum_j q\phi(\mathbf{r}_i, \mathbf{r}_j) + \sum_i q\psi(\mathbf{r}_i)$$

space-charge Coulomb potential

external focusing/acceleration

$$\frac{d\mathbf{r}_i}{ds} = \frac{\partial H}{\partial \mathbf{p}_i}$$

$$\frac{d\mathbf{p}_i}{ds} = -\frac{\partial H}{\partial \mathbf{r}_i}$$

$$\frac{d\zeta}{ds} = -[H, \zeta]$$

A formal single step solution

$$\zeta(\tau) = \exp(-\tau(:H:))\zeta(0)$$

H = H₁+H₂

$$\zeta(\tau) = \exp(-\tau(:H_1: + :H_2:))\zeta(0)$$
$$= \exp(-\frac{1}{2}\tau :H_1:)\exp(-\tau :H_2:)\exp(-\frac{1}{2}\tau :H_1:)\zeta(0) + O(\tau^3)$$

$$\zeta(\tau) = \mathcal{M}(\tau)\zeta(0)$$
$$= \mathcal{M}_1(\tau/2)\mathcal{M}_2(\tau)\mathcal{M}_1(\tau/2)\zeta(0)$$

$\mathcal{M}$ would be symplectic if both $\mathcal{M}_1$ and $\mathcal{M}_2$ are symplectic

J. Qiang, Phys. Rev. Accel. Beams 20, 014203 (2017).

A Symplectic Multi-Particle Tracking Model (2)

$$H_1 = \sum_i \mathbf{p}_i^2/2 + \sum_i q\psi(\mathbf{r}_i) \longrightarrow \mathcal{M}_1$$

- symplectic map for H_1 can be found from charged particle optics method

$$H_2 = \frac{1}{2}\sum_i \sum_j q\phi(\mathbf{r}_i, \mathbf{r}_j) \longrightarrow \mathcal{M}_2$$

$$\mathbf{r}_i(\tau) = \mathbf{r}_i(0)$$

$$\mathbf{p}_i(\tau) = \mathbf{p}_i(0) - \frac{\partial H_2(\mathbf{r})}{\partial \mathbf{r}_i}\tau$$

$$M_2 = \begin{pmatrix} I & 0 \\ L & I \end{pmatrix}$$

To satisfy the symplectic condition: $L = L^T$

$$L_{ij} = \partial \mathbf{p}_i(\tau)/\partial \mathbf{r}_j = -\frac{\partial^2 H_2(\mathbf{r})}{\partial \mathbf{r}_i \partial \mathbf{r}_j}\tau$$

$\mathcal{M}_2$ would be ***symplectic*** if p_i is updated from H_2 ***analytically***

Self-Consistent Space-Charge Transfer Map (1)

$$\frac{\partial^2 \phi}{\partial x^2} + \frac{\partial^2 \phi}{\partial y^2} = -\frac{\rho}{\epsilon_0}$$

$$\begin{aligned} \phi(x=0,y) &= 0 \\ \phi(x=a,y) &= 0 \\ \phi(x,y=0) &= 0 \\ \phi(x,y=b) &= 0 \end{aligned}$$

$$\rho(x,y) = \sum_{l=1}^{N_l}\sum_{m=1}^{N_m} \rho^{lm} \sin(\alpha_l x)\sin(\beta_m y)$$

$$\rho^{lm} = \frac{4}{ab}\int_0^a\int_0^b \rho(x,y)\sin(\alpha_l x)\sin(\beta_m y)\,dxdy$$

$$\phi(x,y) = \sum_{l=1}^{N_l}\sum_{m=1}^{N_m} \phi^{lm} \sin(\alpha_l x)\sin(\beta_m y)$$

$$\phi^{lm} = \frac{4}{ab}\int_0^a\int_0^b \phi(x,y)\sin(\alpha_l x)\sin(\beta_m y)\,dxdy$$

$$H_2 = 4\pi\frac{K}{2}\frac{4}{ab}\frac{1}{N_p}\sum_{i=1}^{N_p}\sum_{j=1}^{N_p}\sum_{l=1}^{N_l}\sum_{m=1}^{N_m}\frac{1}{\gamma_{lm}^2}$$

$$\int_0^a\int_0^b S(x-x_j)S(y-y_j)\sin(\alpha_l x)\sin(\beta_m y)dxdy \int_0^a\int_0^b S(x-x_i)S(y-y_i)\sin(\alpha_l x)\sin(\beta_m y)dxdy$$

$$\rho(x_{I'},y_{J'}) = \frac{1}{N_p}\sum_{j=1}^{N_p} S(x_{I'}-x_j)S(y_{J'}-y_j),$$

J. Qiang, Phys. Rev. Accel. Beams 21, 054201 (2018).

Symplectic Gridless Particle Model

$$\rho(x,y) = \sum_{j=1}^{N_p} w\delta(x-x_j)\delta(y-y_j)$$

w is the particle charge weight

$$H_2 = \frac{1}{2\epsilon_0}\frac{4}{ab} w \sum_i \sum_j \sum_l \sum_m \frac{1}{\gamma_{lm}^2} \sin(\alpha_l x_j) \sin(\beta_m y_j)\sin(\alpha_l x_i)\sin(\beta_m y_i)$$

$\mathcal{M}_2$

$$\begin{aligned} p_{xi}(\tau) &= p_{xi}(0) - \tau \frac{1}{\epsilon_0}\frac{4}{ab} w \sum_j \sum_l \sum_m \frac{\alpha_l}{\gamma_{lm}^2} \\ &\quad \sin(\alpha_l x_j)\sin(\beta_m y_j)\cos(\alpha_l x_i)\sin(\beta_m y_i) \\ p_{yi}(\tau) &= p_{yi}(0) - \tau \frac{1}{\epsilon_0}\frac{4}{ab} w \sum_j \sum_l \sum_m \frac{\beta_m}{\gamma_{lm}^2} \\ &\quad \sin(\alpha_l x_j)\sin(\beta_m y_j)\sin(\alpha_l x_i)\cos(\beta_m y_i) \end{aligned}$$

Symplectic Particle-In-Cell Model

$\mathcal{M}_2$ →

$$p_{xi}(\tau) = p_{xi}(0) - \tau 4\pi K \sum_I \sum_J \frac{\partial S(x_I - x_i)}{\partial x_i} S(y_J - y_i)\phi(x_I, y_J)$$

$$p_{yi}(\tau) = p_{yi}(0) - \tau 4\pi K \sum_I \sum_J S(x_I - x_i)\frac{\partial S(y_J - y_i)}{\partial y_i}\phi(x_I, y_J)$$

$$\phi(x_I, y_J) = \frac{4}{ab}\sum_{l=1}^{N_l}\sum_{m=1}^{N_m}\frac{1}{\gamma_{lm}^2}\sum_{I'}\sum_{J'}\rho(x_{I'}, y_{J'})\sin(\alpha_l x_{I'})\sin(\beta_m y_{J'})\sin(\alpha_l x_I)\sin(\beta_m y_J)$$

$$S(x_I - x_i) = \frac{1}{h}\begin{cases} \frac{3}{4} - (\frac{x_i - x_I}{h})^2, & |x_i - x_I| \le h/2 \\ \frac{1}{2}(\frac{3}{2} - \frac{|x_i - x_I|}{h})^2, & h/2 < |x_i - x_I| \le 3/2h \\ 0 & \text{otherwise} \end{cases}$$

$$\frac{\partial S(x_I - x_i)}{\partial x_i} = \begin{cases} -2(\frac{x_i - x_I}{h})/h, & |x_i - x_I| \le h/2 \\ (-\frac{3}{2} + \frac{(x_i - x_I)}{h})/h, & h/2 < |x_i - x_I| \le 3/2h, \quad x_i > x_I \\ (\frac{3}{2} + \frac{(x_i - x_I)}{h})/h, & h/2 < |x_i - x_I| \le 3/2h, \quad x_i \le x_I \\ 0 & \text{otherwise} \end{cases}$$

Significant Difference in Final 4D Emittances Between the Symplectic and the Non-Symplectic Methods (Strong Space-Charge: Phase Advance Change 85 -> 42)

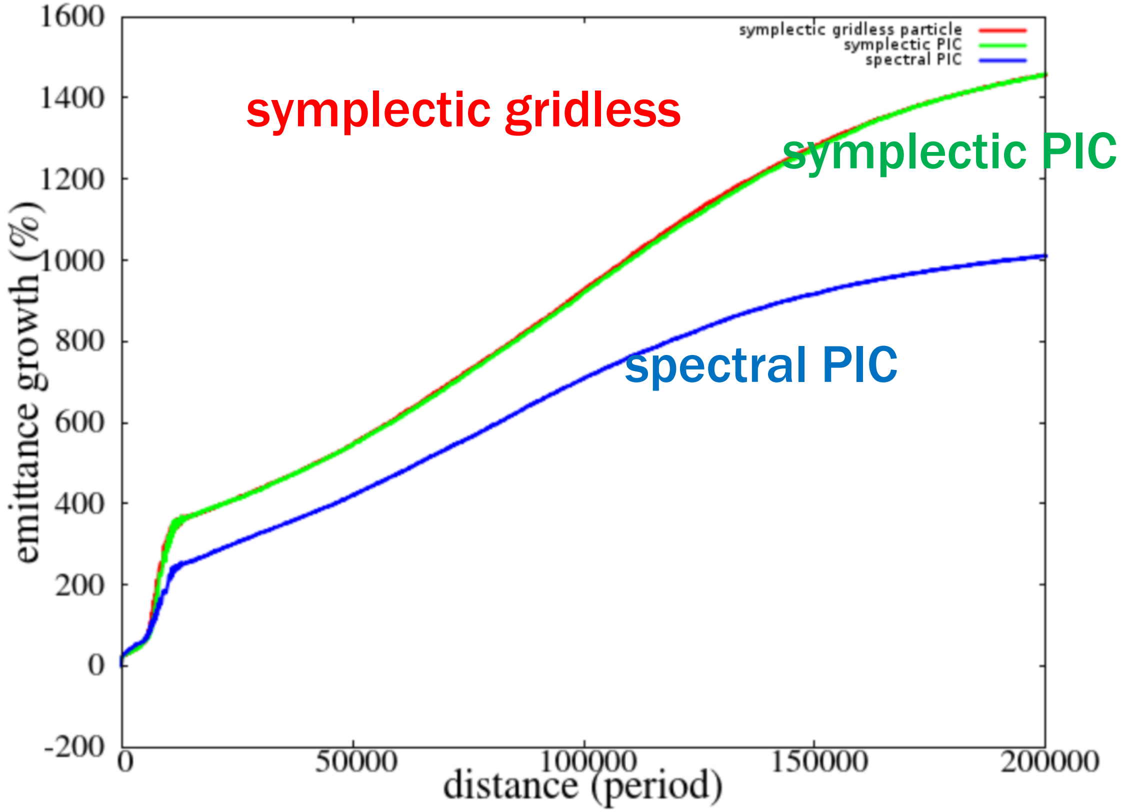

Two symplectic approaches show good agreement.

Finer Step Size Needed for Non-Symplectic PIC (Symplectic PIC vs. Non-Symplectic PIC)

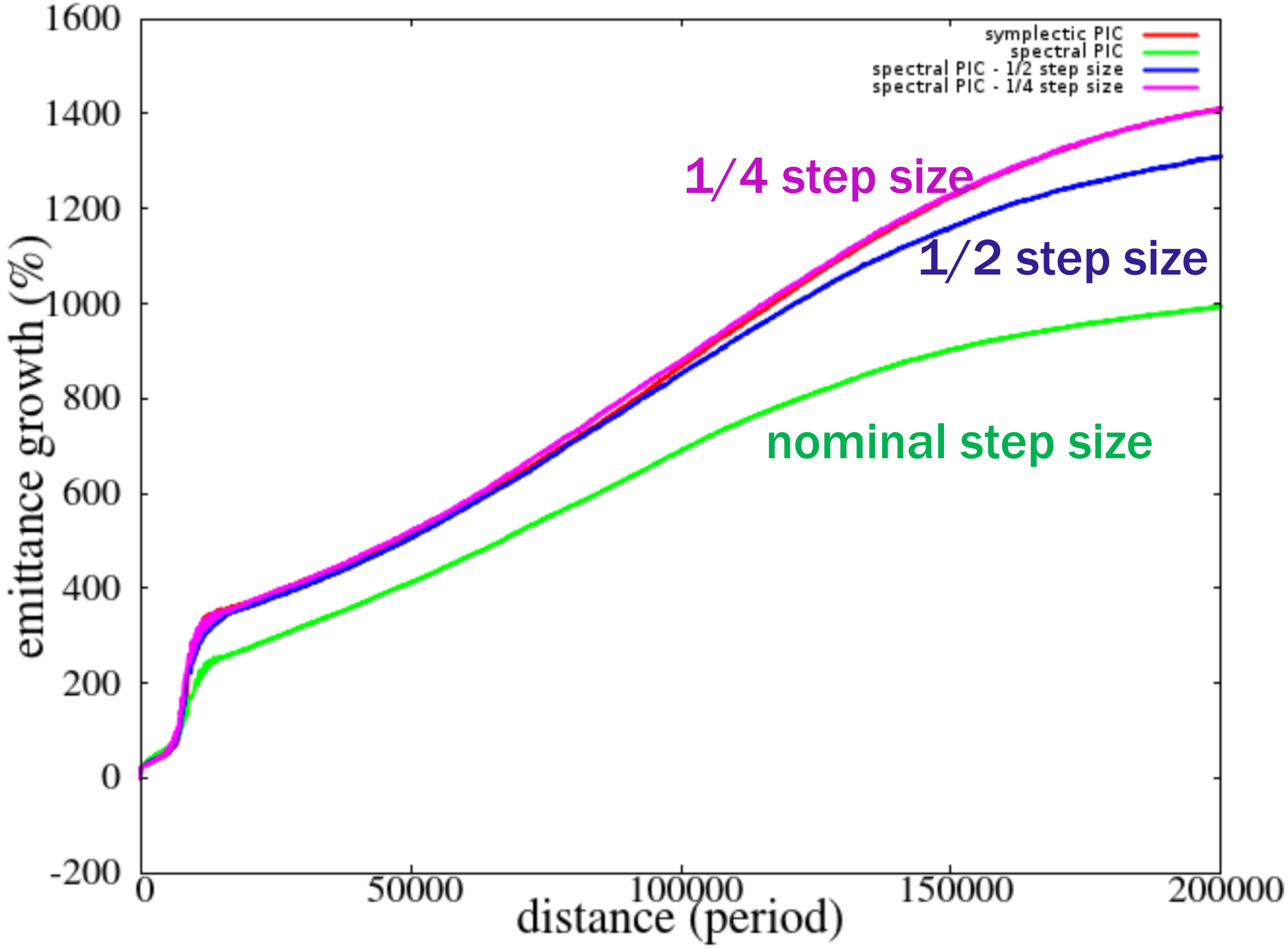

Long Term Space-Charge Tracking in an Ideal Ring
1 Turn = 10 FODOs + 1 Sextupole

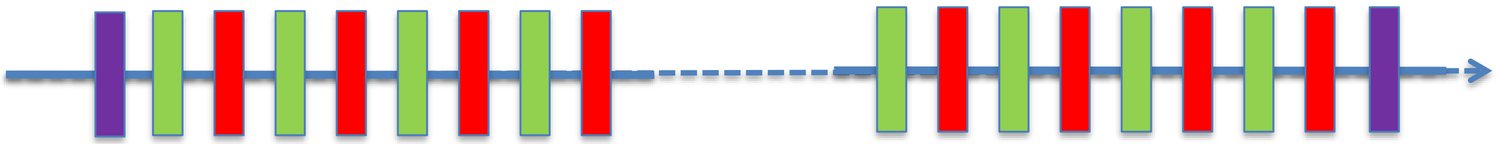

- 0 current tune 2.417, 30 A current, tune shift 0.113
- symplectic PIC model
- 1) sextupole KL = 0
- 2) sextupole KL = 10 T/m/m

BERKELEY LAB

U.S. DEPARTMENT OF ENERGY | Office of Science

ACCELERATOR TECHNOLOGY & APPLIED PHYSICS DIVISION ATAP

Extra Numerical Emittance Growth with Small Number of Macroparticles

sextupole KL = 0, 64x64 modes

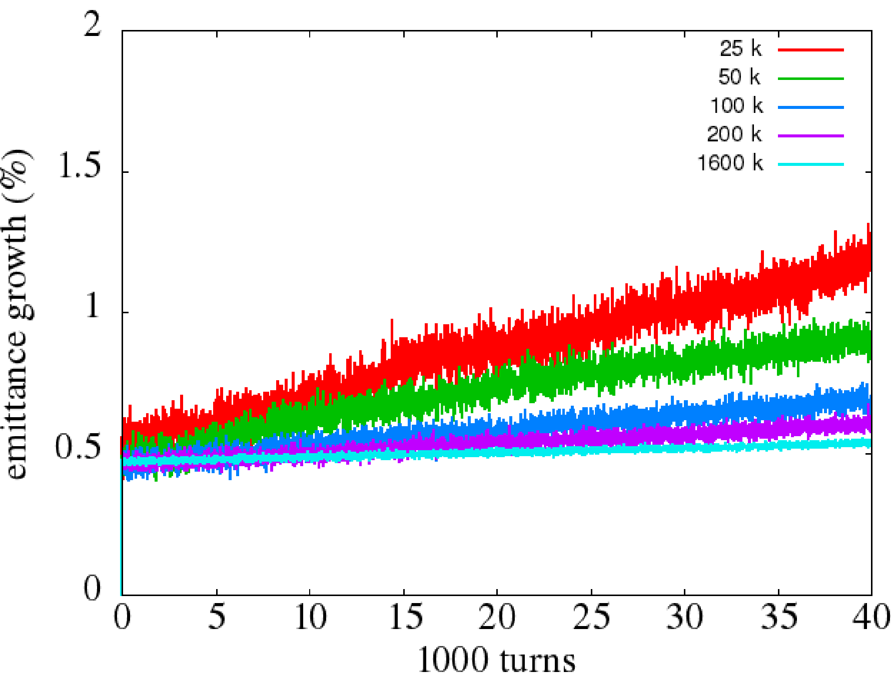

sextupole KL = 10, 64x64 modes

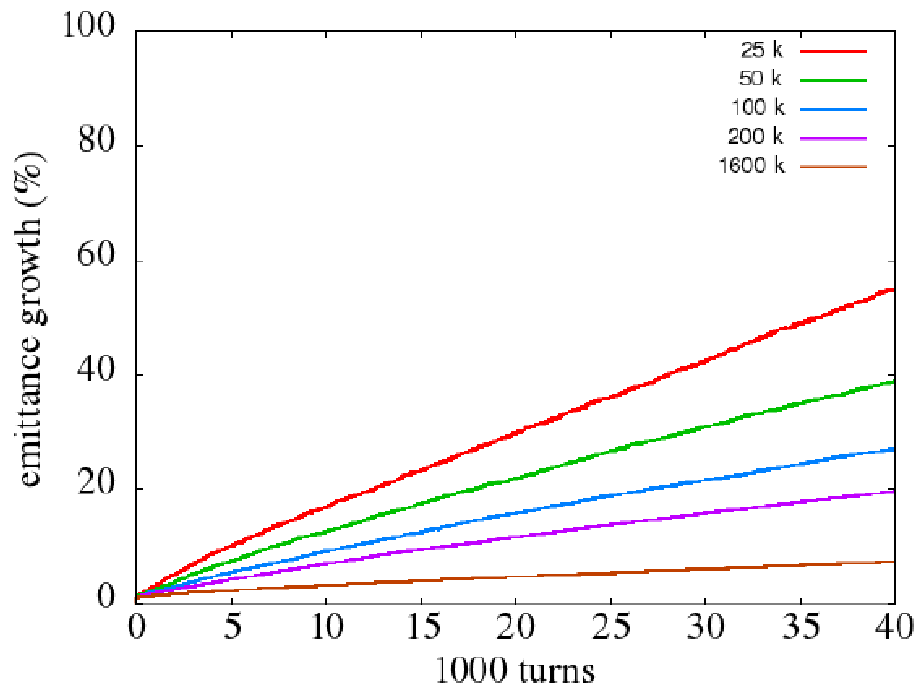

- **Little emittance growth in the linear lattice**
- **Small emittance growth driven by the 3rd order resonance**
- **Sufficient number of macroparticles needed to suppress numerical emittance growth**

Understand the Numerical Emittance Growth from a 1D Model

The *smooth* and the reconstructed Gaussian distributions from macroparticle sampling with *linear*, *quadratic*, and *Gaussian kernel* deposition

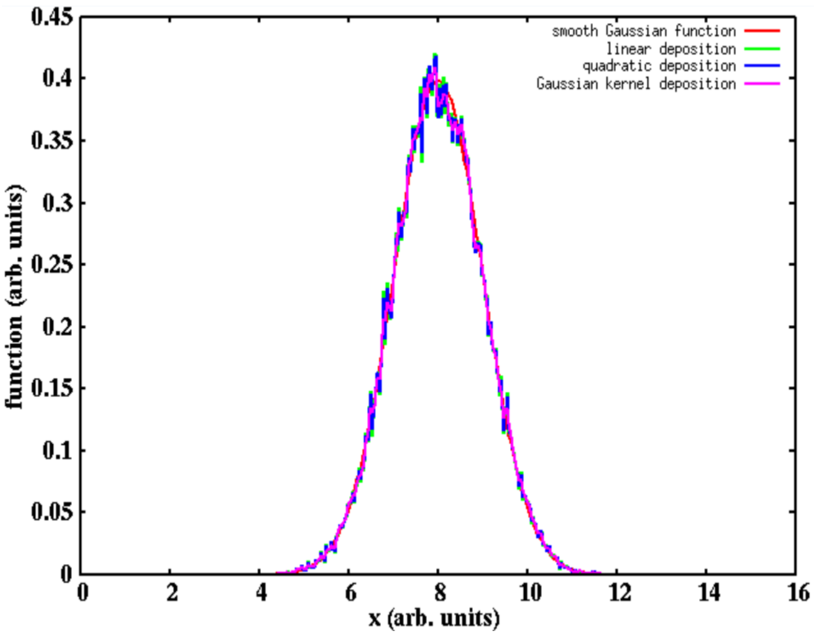

The mode amplitude of the smooth and the reconstructed Gaussian distributions from macroparticle sampling with linear, quadratic, and Gaussian kernel deposition

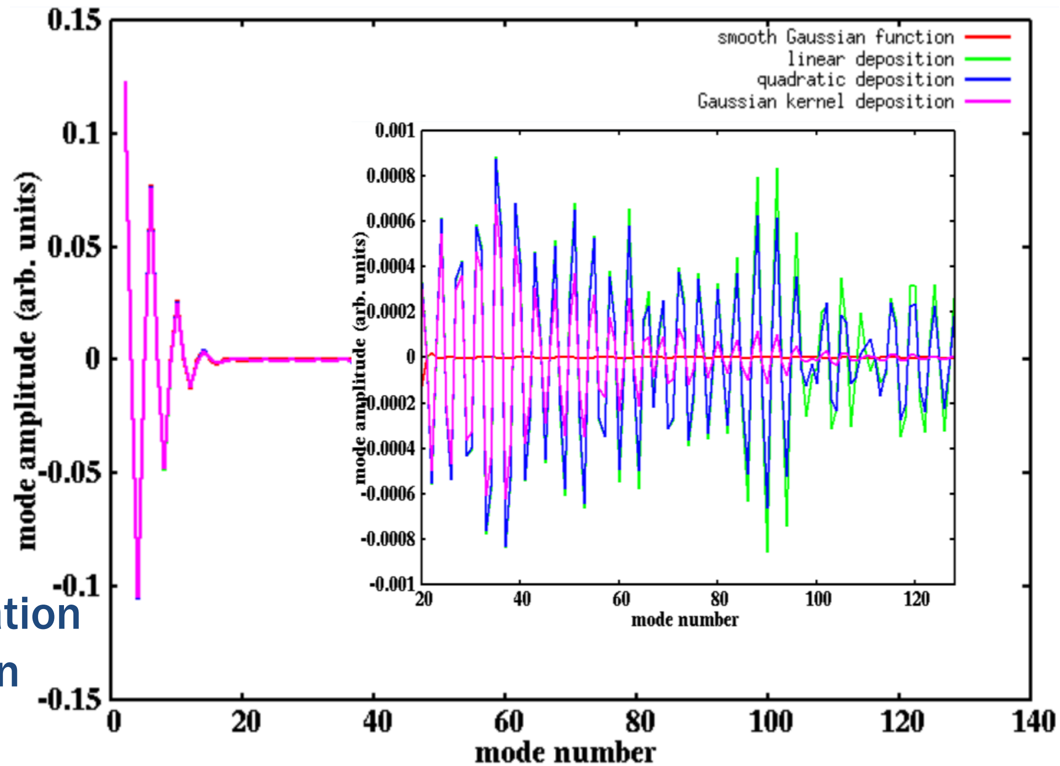

➢ **Much larger mode amplitude fluctuation from the macroparticle depositions than that from the smooth distribution**

Quantify the Mode Amplitude Fluctuation with Standard Deviation

$$\rho^l = \frac{1}{N_p}\frac{2}{N_g\Delta x}\sum_i\sum_I S(x_I - x_i)\sin(\alpha_l x_i)$$

$$var(\rho^l) = \frac{1}{N_p}var(\frac{2}{N_g\Delta x}\sum_I S(x_I - x_i)\sin(\alpha_l x_i))$$

$$var(\frac{2}{N_g\Delta x}\sum_I S(x_I - x_i)\sin(\alpha_l x_i)) \approx \frac{1}{N_p}(\frac{2}{N_g\Delta x})^2\sum_i[\sum_I S(x_I - x_i)\sin(\alpha_l x_i)]^2 - (\rho^l)^2$$

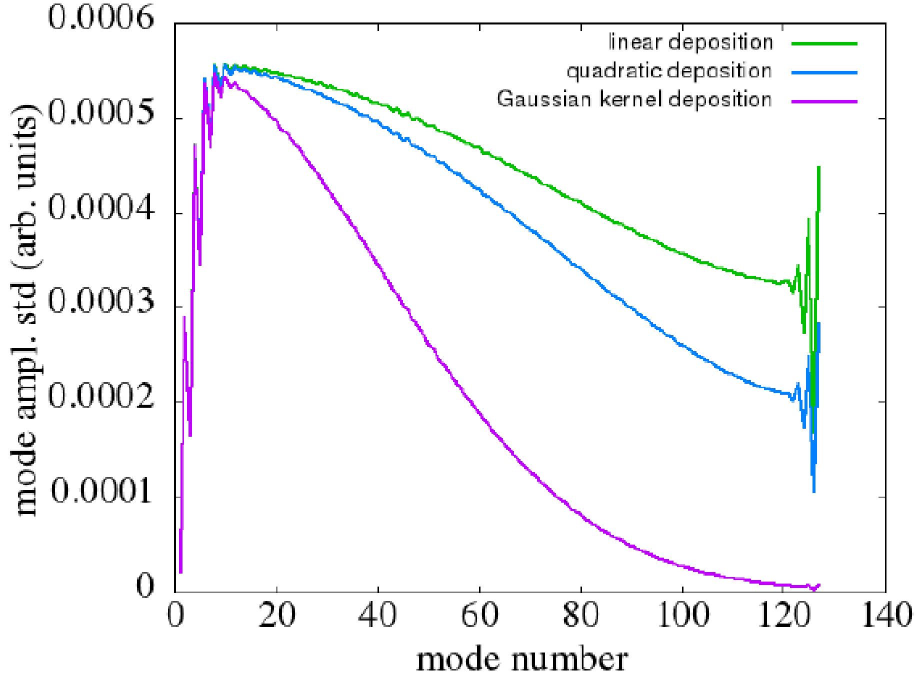

➢ **Higher order macroparticle deposition scheme leads to smaller fluctuation**

Mode Amplitude Fluctuation Decreases with the Increase of Macroparticle Number

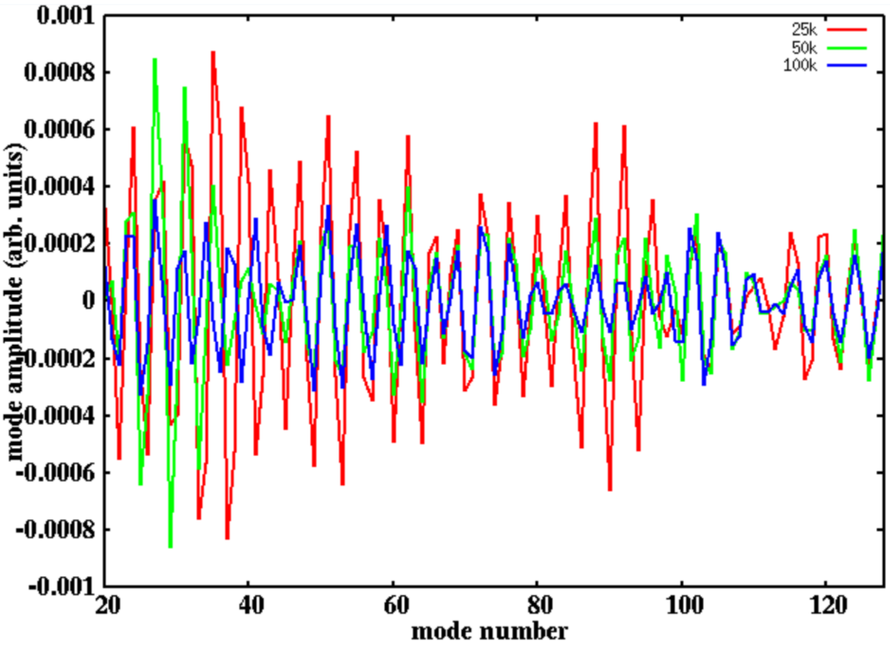

- Fluctuation standard deviation ~ 1/sqrt(Np)

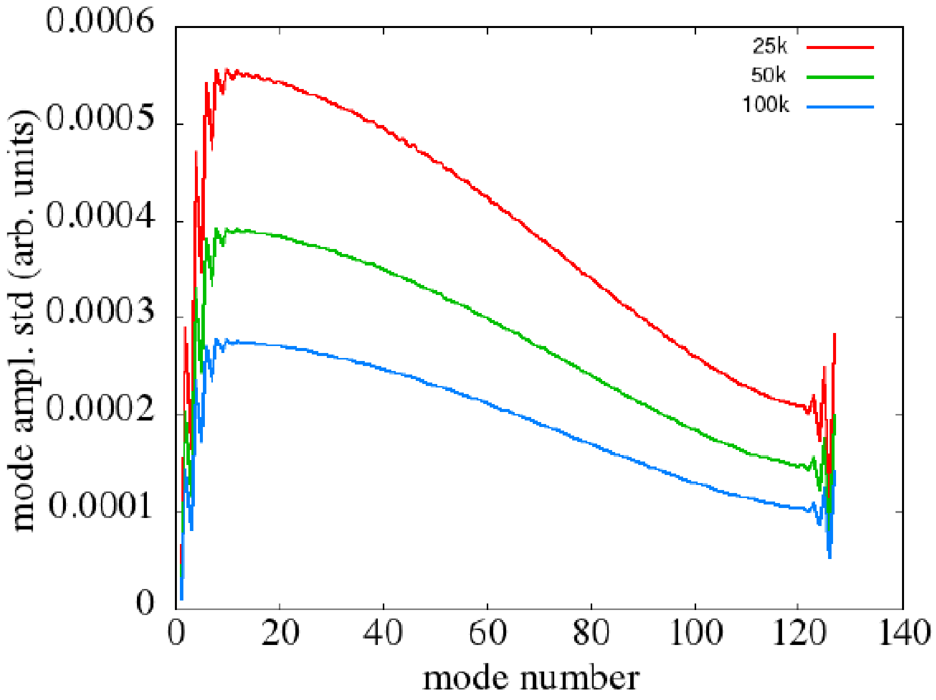

Mode Amplitude Fluctuation Increases with the Increase of Grid Number

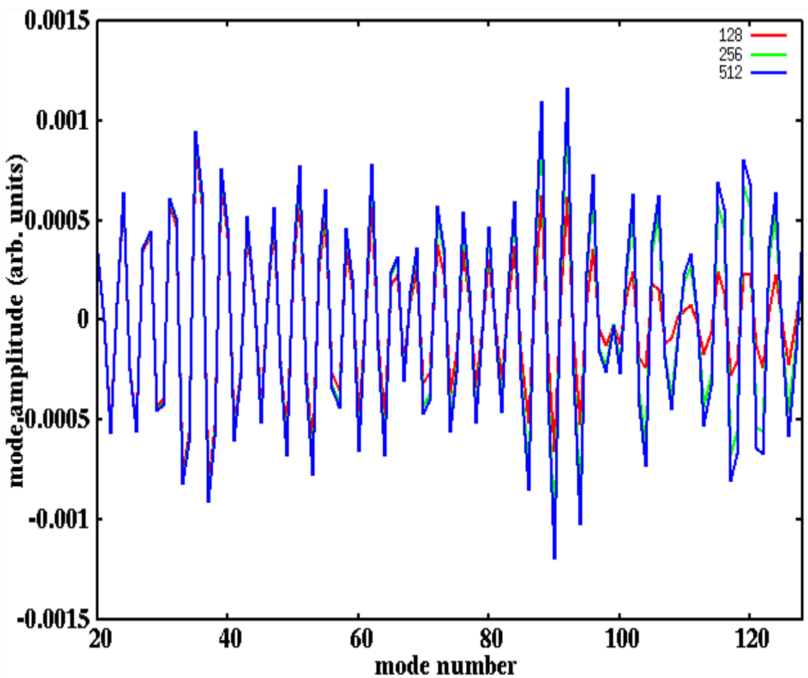

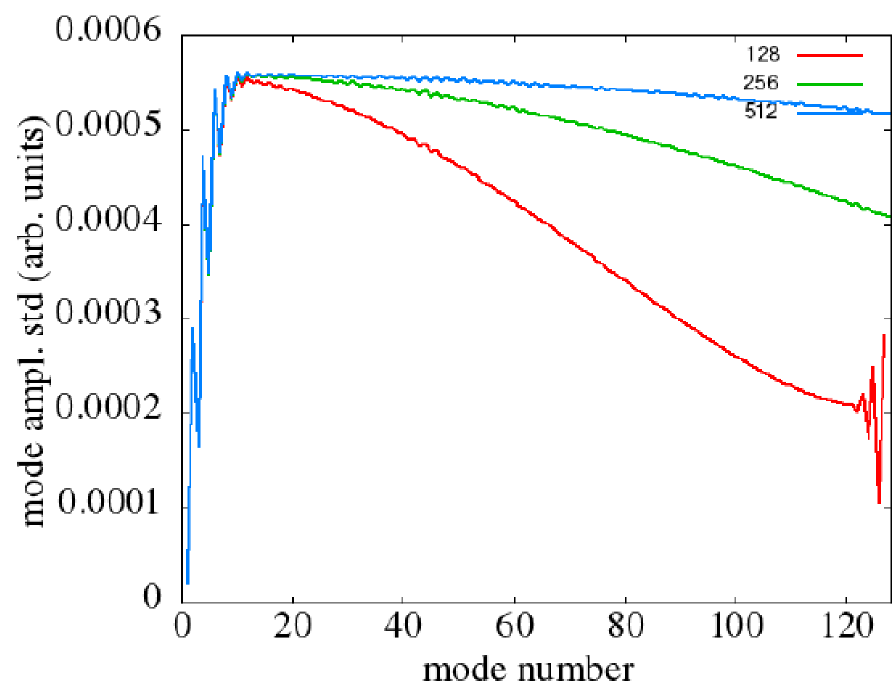

- Grid number mainly affects mode number > 10
- Larger grid number results in larger fluctuation

Numerical Errors of in the Charge Density Distribution from Macroparticles Results in Numerical Emittance Growth

$$\Delta\epsilon \approx (<x^2><x'\delta F> - <xx'><x\delta F>)\tau/\epsilon + \frac{1}{2}(<x^2><(\delta F)^2> - <x\delta F>^2)\tau^2/\epsilon$$

$$\frac{\Delta\epsilon}{\tau} \approx \frac{1}{2}<x^2><(\delta F)^2>\tau/\epsilon$$

sextupole KL = 0, 64x64 modes

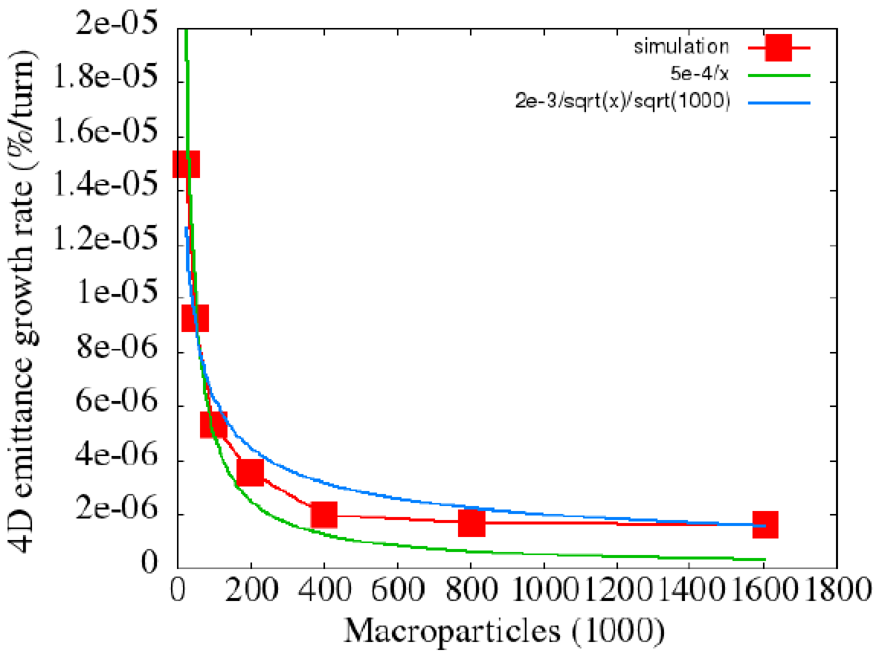

- Numerical emittance growth scales between 1/Np and 1/sqrt(Np)

sextupole KL = 10, 64x64 modes

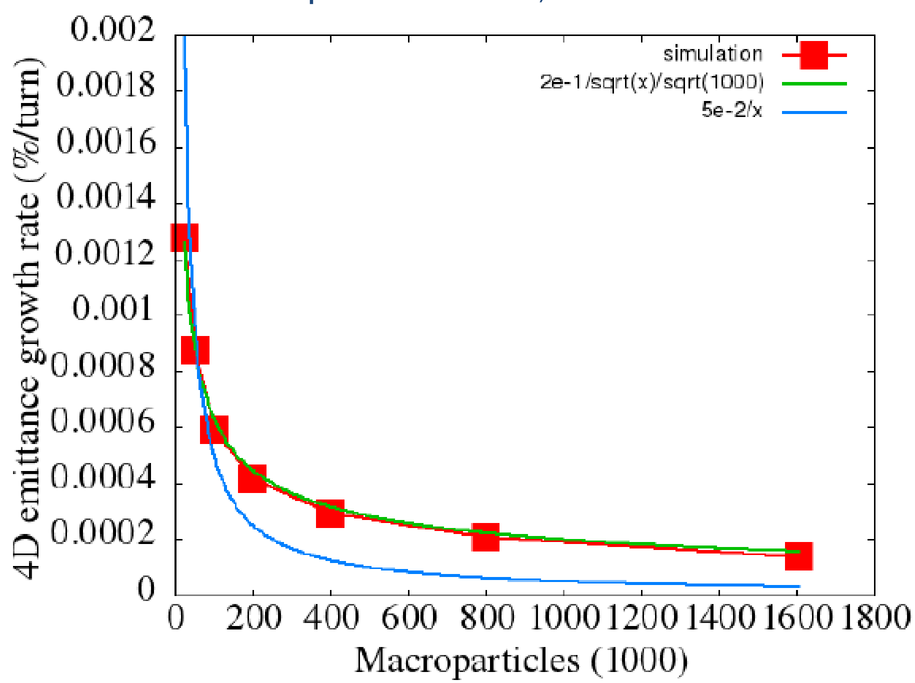

- Numerical emittance growth scales close to 1/sqrt(Np)
- The growth mechanism is more complicated

Removing Small Amplitude Fluctuation Modes Using Relative Amplitude Threshold (1)

Spectral amplitude of a 2D Gaussian density (64x64 mode)

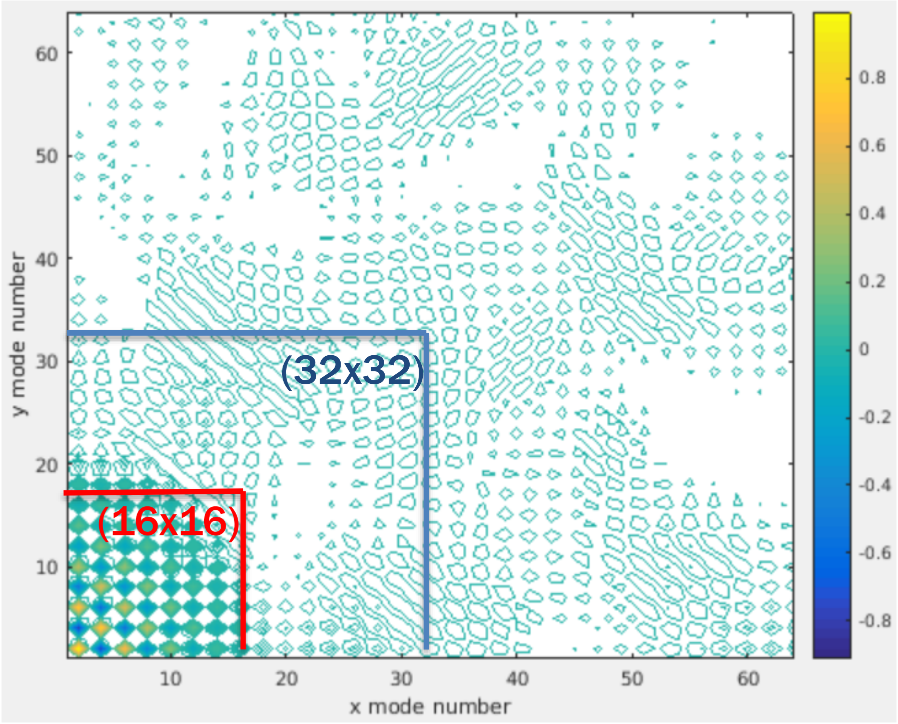

Spectral amplitude of a 2D Gaussian density with 1% threshold

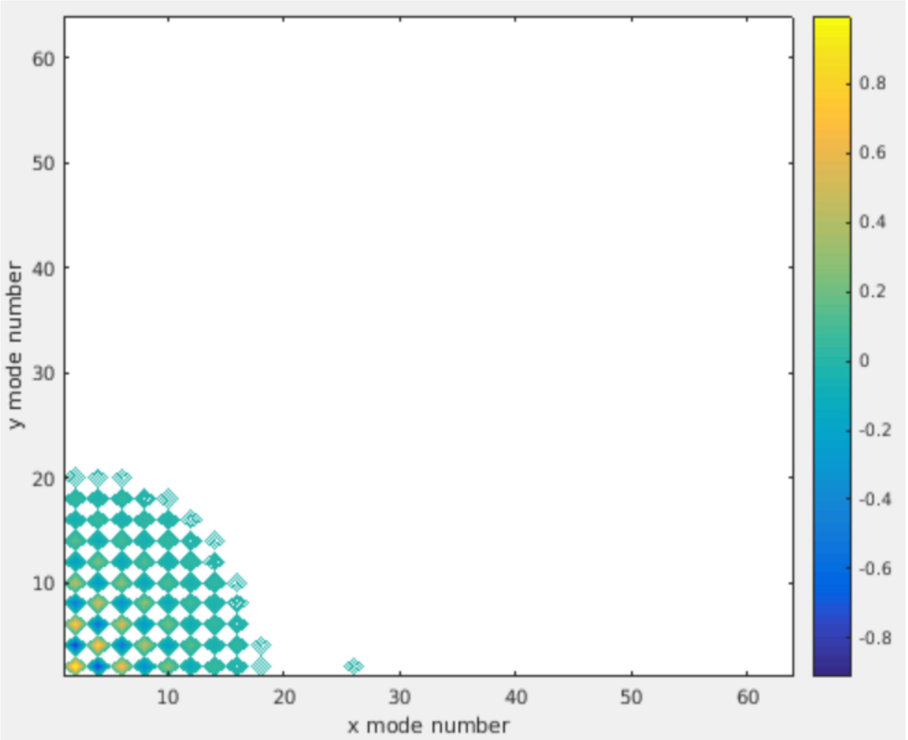

Removing Small Amplitude Fluctuation Modes Using Relative Amplitude Threshold (2)

Spectral amplitude of a 2D Gaussian density with 2 sigma threshold

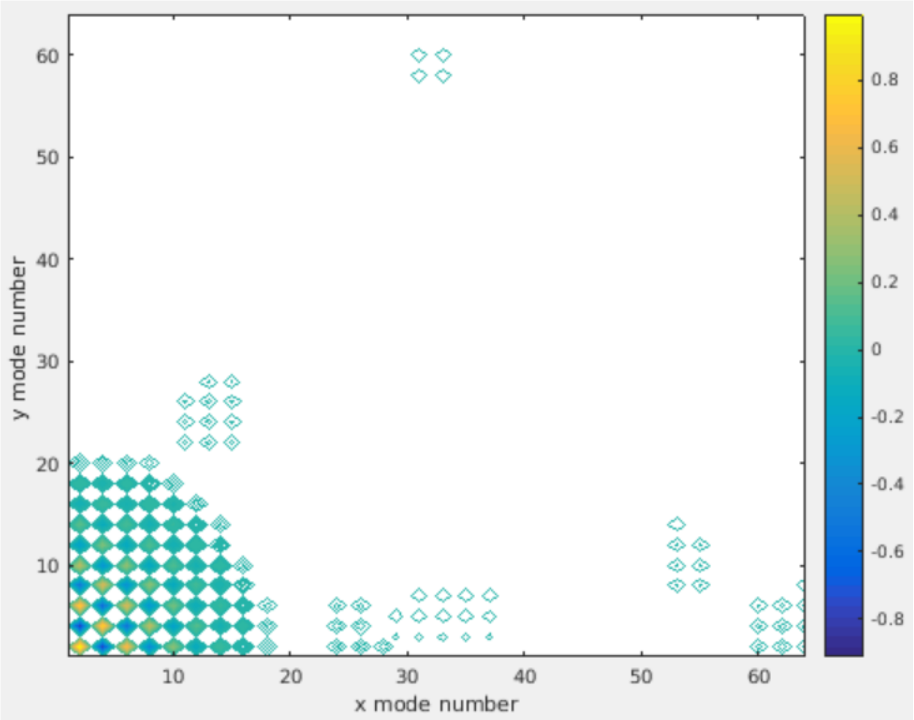

Spectral amplitude of a 2D Gaussian density with 4 sigma threshold

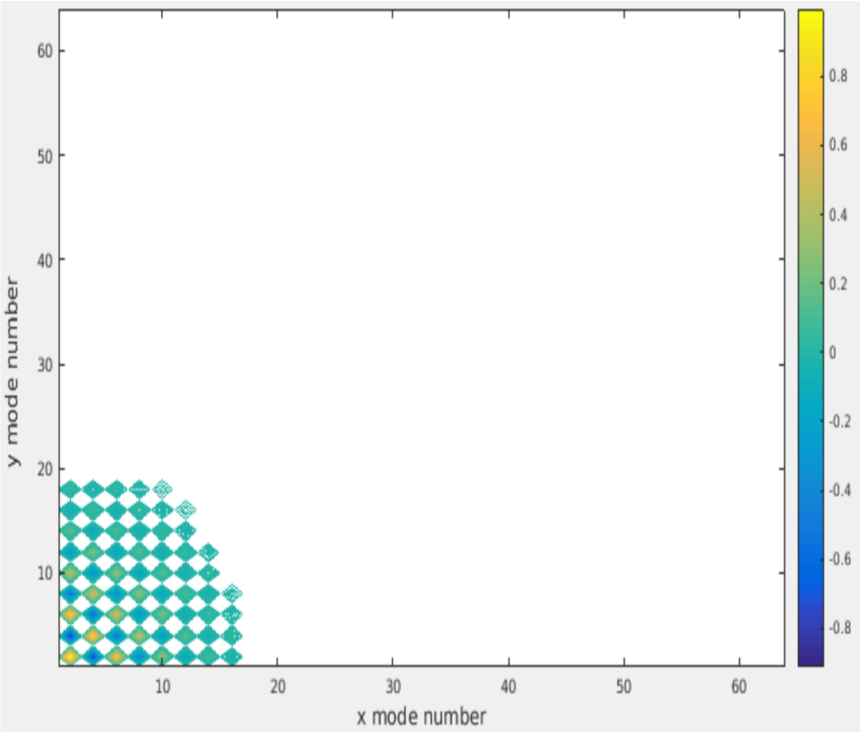

Mitigate the Numerical Emittance Growth by Removing High Frequency Modes in Linear Lattice

sextupole KL = 0, current = 30 A, 25 k macroparticles

brute force cut-off

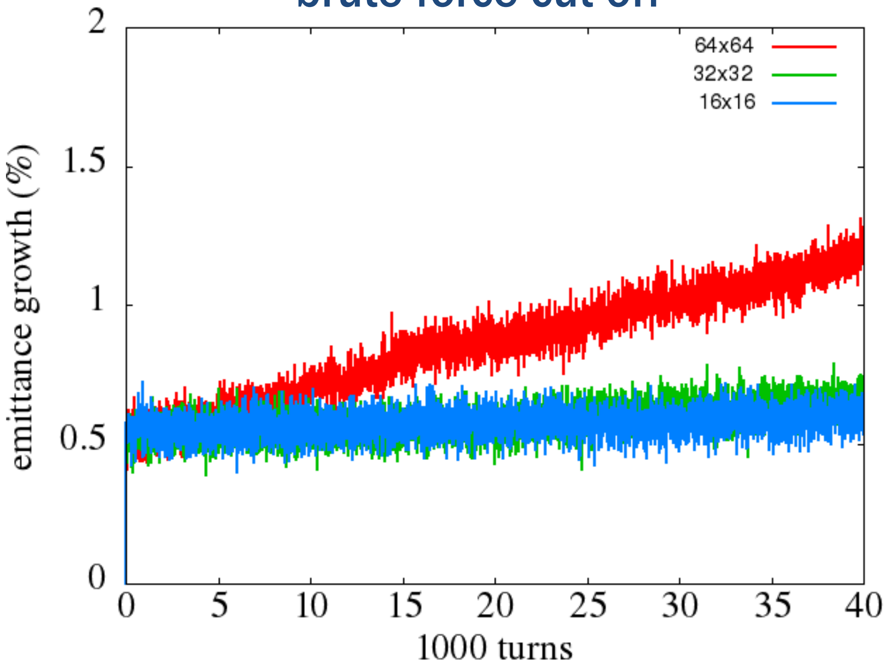

threshold filtering

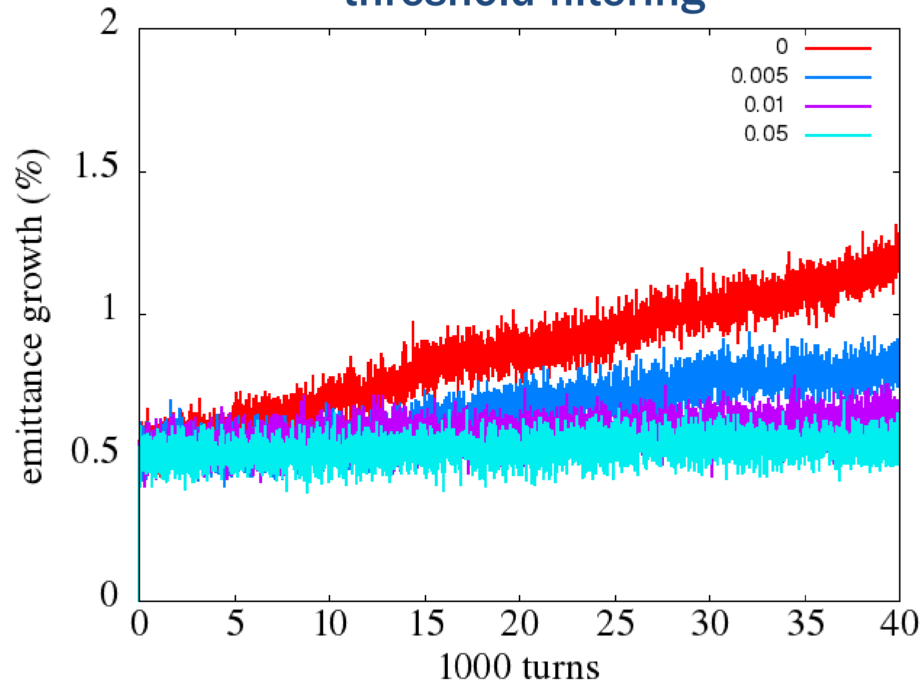

- Both numerical filters work well
- Numerical emittance growth is mainly due high frequency errors

Mitigate the Numerical Emittance Growth through Threshold Filtering in Nonlinear Lattice

sextupole KL = 10, current = 30 A, 25 k macroparticles

brute force cut-off

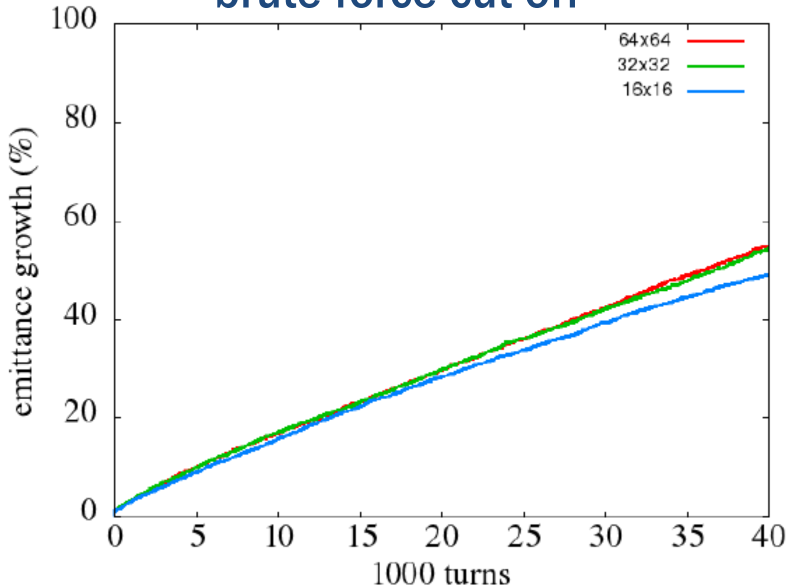

threshold filtering

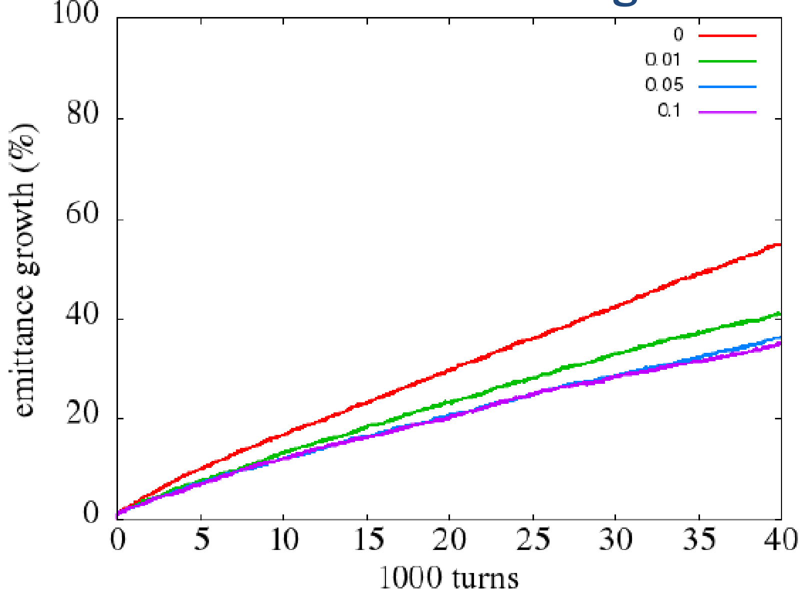

- Direct brute force cut-off filtering is not efficient
- Numerical emittance growth can be mitigated with threshold filtering
- The numerical growth is mainly due low frequency errors

Predefined Maximum Fraction and Four Sigma Threshold Filtering Yields Similar Emittance Growth

sextupole KL = 10, current = 30 A, 25 k macroparticles

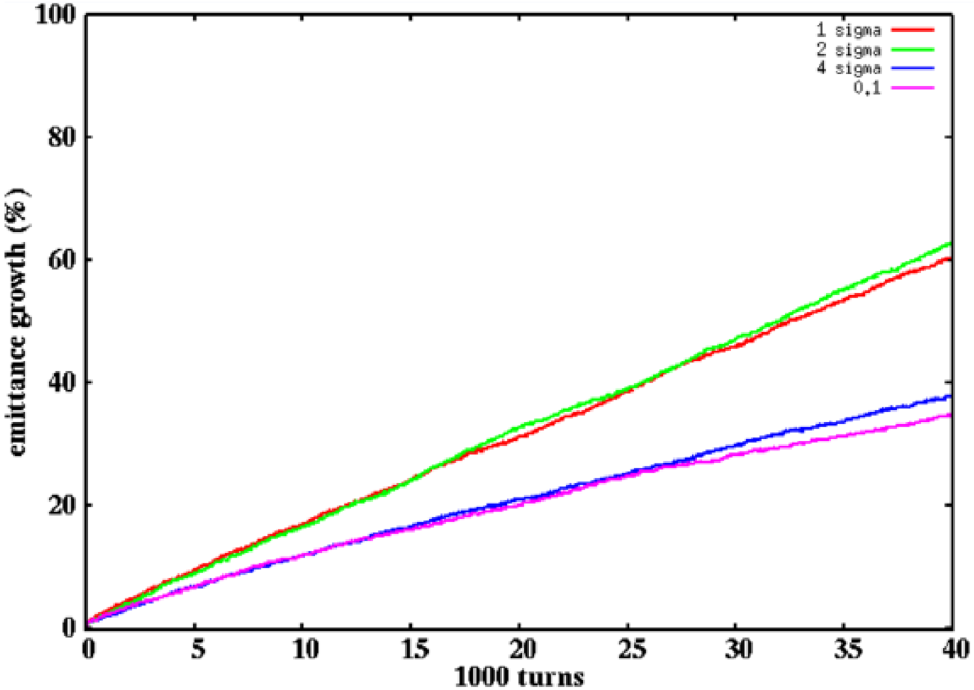

Maximum Fraction

Pro – easy to calculate the threshold value

Con – another hyperparameter

Standard Deviation

Pro – calculate the threshold value dynamically

Con – computationally expensive

Summary

- **Simulation of high brightness electron beams:**
  - start-to-end simulation of LCLS uBI experiment showed good agreement between the simulations and the measurements
  - start-to-end global optimization improves the final beam brightness

- **Simulation of high intensity proton beams:**
  - symplectic space-charge model will help improve the accuracy of simulation
  - numerical emittance growth from finite macroparticle sampling can be mitigated using threshold filtering in frequency domain

Thank You!